Iraqi Journal of Veterinary Sciences

www.vetmedmosul.com

The combined effect of the human umbilical cord blood with chitosan scaffold on the full-thickness wound healing process in rats

A.J. El-Shaer[1], A.A. Abuel-atta[1], H.A. Badr[2] and D.A. AlSadek[1]

[1]Department of Histology and Cytology, Faculty of Veterinary Medicine, [2]Department of Biochemistry, Faculty of Agriculture, Zagazig University, Zagazig, Egypt

Article information

Article history:
Received July 21, 2022
Accepted November 27, 2022
Available online February 24, 2023

Keywords:
Scaffolds
Tissue engineering
Plant lectins
Mast cells
Skin regeneration

Correspondence:
A.J. El-Shaer
elshaer.aida@yahoo.com

Abstract

This study aimed to investigate the role of a low dose of human umbilical cord blood mesenchymal stem cells (HUCB-MSCs) with chitosan scaffold (ChSc) on the progress of the cutaneous wound healing process in male Albino rats. A full-thickness cutaneous wound with a circular shape with a diameter of about 2 cm was induced on the dorsum of thirty-six Albino male rats, divided into four groups: the first group, the wounds were left without treatment as a control group. In the second group, the wounds were covered by freeze-dried ChSc. While in the third group, the wounds were treated through injection of the HUCB-MSCs intradermally, and in the fourth group, the ChSc seeded with HUCB-MSCs were used together to treat the wounds. The progress of wound healing was monitored by histological, immunohistochemical, and biochemical assays for all experimental groups at 3, 8, and 21 postoperative days. Both ChSc and the low dose of HUCB-MSCs alone performed moderate healing progress. The (HUCB-MSCs) ChSc group exhibited an increased healing rate more than the other groups and reported an appropriate collagen deposition without scarring signs, effective mast cell regulation, and well vascularization. In conclusion, the fourth group (the HUCB-MSCs with ChSc) improved the healing process, revealing the highest healing rate and performance without complications.

DOI: 10.33899/ijvs.2022.134782.2404,

Introduction

Open wounds may find difficulty in normal healing processes because they can be infected by microorganisms or cannot be healed appropriately without scar or fibrotic tissue formation leading to tissue necrosis (1). Wounds can occur by various factors, including trauma, surgeries, cuts, pressure, and burns (2). The wound is damage that results in injury to the skin. The wound healing process consists of stages: hemostasis, inflammation, proliferation, and remodeling. It was found that the healing cascade of healing stages is interpreted during severe wounds, which might result in tissue necrosis through the second infection (3). Open excised wounds did not close spontaneously due to loss of contact between the edges. Connection of the wound edges with medical glue, clips, or sutures helps the edges get in touch and heal together by primary intention. However, not all incised wounds close by the primary intention mechanism due to excessive tissue loss and the risk of infection that delays the normal healing process. The full-thickness open wound is usually healed by secondary intention (4). Therefore, the dressings used to treat skin wounds must be non-toxic, antibacterial, biocompatible, mucoadhesive, regulated degradation rate, and cost-effective (5). Chitosan is a polysaccharide consisting of glucose amine polymer prepared by deacetylation of chitin, the second most abundant natural polymer after cellulose (6,7). Chitosan is extracted from the crustacean's exoskeleton, considered the primary source of chitosan, then the insects and the fungal cell wall (8). Chitosan has several properties which make it

desirable in many medical applications, such as a good solubilization rate which facility producing different pharmaceutical products, such as powders, films, membranes, hydrogels, or paste (9,10). Chitosan processes an adhesive property that encourages the direct application of chitosan to open wounds (11). Skin substitutes are named biological skin substitutes, bio-engineered skin, tissue-engineered skin, bio-constructs, artificial skin (12), and scaffolds (13,14). Skin substitutes are applied for tissue or organ regeneration and replacement *in vivo* (13). Chitosan scaffold (ChSc) has a high capacity to absorb wound exudate, which keeps the ChSc flexible, and also, the interconnected porous structure of the ChSc offers good cellular interaction and migration that promote tissue regeneration (15). There are different sources of the mesenchymal stem cells (MSCs) such as bone marrow-derived mesenchymal stem cells (BM-MSCs) (16), adipose derived mesenchymal stem cells (ADMSCs) (17), placenta derived mesenchymal stem cells (PMSCs) (18), Multipotent mesenchymal stromal cells (MSCs) (19), and the human umbilical cord blood mesenchymal stem cells (HUCB-MSCs) (17). The HUCB-MSCs have the potency to regenerate damaged skin tissue (20). Eylert *et al.* (16) reported that adminestring a low number of BM-MSCs in a pig model enhanced healing compared to the higher applied dose. The HUCB-MSCs participate in immunoregulation, such as the down-regulation of pro-inflammatory cytokines and inflammatory cells (20). Therefore, stem cells were preferable in grafting therapy (21). Mast cells are tissue-specific immune cells that originate from the bone marrow and are in high numbers in external tissues such as the skin (22). In addition, when tissue mismatches with the grafted foreign body, the mast cell initiates an inflammatory response and increases collagen deposition by activating the fibroblasts. This mechanism resulted in fibrotic tissue where a fibrous capsule formed around the graft and stimulated tissue rejection response (23).

This study investigates the combined impact of freeze-dried ChSc when seeded with a low number of HUCB-MSCs in enhancing the wound healing process and regulating mast cells' response against the implanted scaffold and human stem cells in a rat model.

Materials and methods

Ethical approve

The experimental procedures were performed according to the Laboratory Animal Care and Use Regulations guidelines and approved by the Research Ethics Committee of Zagazig University, Egypt (Approval No: ZU-IACUCl/2/F/46/2020).

Experimental animals

The experiment was performed on 36 male Wister albino rats that weighed 200-250 gm. The rats were housed in individual cages in the animal house for about one week at a controlled temperature 25-30ºC and fed water to adapt the animals to the environment before being experimented.

Isolation of HUCB-MSCs

Human umbilical cord blood (HUCB) was collected and isolated from the umbilical cord as described by Secunda *et al.* (17). In brief, the HUCB was collected in a sterile tube with heparin 1000 units (EMC, UK) as an anticoagulant. Phosphate-buffered saline (PBS/2mM EDTA) (Lonza Bioproducts, Belgium) was used to dilute the HUCB in 1:2 ratios. Then an equal volume of Ficoll-paque® (Lonza Bioproducts, Belgium) was added carefully to the diluted HUCB. After centrifuging for 20 min at 2400 rpm at 20°C, the layer containing stem cells and white blood corpuscles (WBCs) was collected, then transferred into another sterile tube that was washed twice with sterile (PBS/2 mM EDTA) (Lonza Bioproducts, Belgium). Then cultured into T25 culture flasks (Falcon, Becton Dickinson, Heidelberg, Germany) with serum-free Dulbecco′s modified Eagle′s medium (DMEM) (Lonza Bioproducts, Belgium) supplemented with 10% fetal bovine serum (FBS) (Lonza Bioproducts, Belgium) in sterile conditions, then incubated in a 5% CO_2 incubator at 37°C (Heraeus, Langenselbold, Germany). The HUCB-MSCs attached to the culture flask wall reached 80% confluence by the third passage. Cultures were washed twice with (PBS/2 mM EDTA) (Lonza Bioproducts, Belgium) and trypsinized with 0.25% trypsin/EDTA (Lonza Bioproducts, Belgium) for 10 min at 37°C. Afterward, the cells were centrifugated at 2400 rpm for 20 min. Finally, the cells were suspended in DMEM with 10% FBS, then divided into 3 x 10^5 cells per 500 µL for each dose (17).

Immunophenotypic characterization of HUCB-MSCs

The HUCB-MSCs were trypsinized after the 3rd passage of the culture, then 500,000 cells were incubated with 20µl of specific monoclonal antibodies CD105 and $CD34^-$ 20µl (BD Bioscience), and mouse isotype-matched IgG (BD Pharmingen) as a negative control for 30 minutes in the dark. Then washed with 250 µl of Phosphate buffered saline according to the instructions of the technique and detected by a FACS flow cytometer (Becton Dickinson, Heidelberg, Germany) running Cell Quest software (BD, San Joe, USA). Only 20,000 labeled cells were acquired and analyzed. The anti-CD105 monoclonal antibody detects the mesenchymal-specific surface marker, and the anti-$CD34^-$monoclonal antibody detects hematopoietic stem cells (24).

ChSc preparation characterization

The scaffold was manufactured from chitosan powder (Chitosan-Egypt®). The chitosan was 90% ± 5 deacetylated, with a viscosity of 250 cps. Two grams of chitosan powder were dissolved in 2 % glacial acetic acid (Sigma-Aldrich, USA) with heating. The prepared chitosan hydrogel was

poured into a flat container and frozen at -80 °C overnight. The frozen chitosan hydrogel was freeze-dried in a lyophilizer (Christ, Alpha 1-4 LSC plus) at -60 °C under a pressure of 0.001 mbar for 18 hours. The yielded freeze-dried ChSc was cut into 2 cm diameter circle-shaped pieces. The circle-shaped ChSc was cross-linked and sterilized by immersion in gradient descending concentrations of ethyl alcohol (Sigma-Aldrich, USA), 95%, 85%, and 75%, respectively, for 20 minutes (25).

Characterization of ChSc using scanning electron microscopy (SEM)

The ChSc was coated with gold (Au) and then examined by SEM (JSM-6510, Jeol Ltd., Japan) at 30 kV. The images were taken using the SEM software (JEM-2100F, Jeol Ltd., Japan), and the attached digital camera was used to analyze the surface properties of the ChSc and determine its porous diameter.

Experimental Design

All rats were anesthetized with Thiopental sodium 500 mg (EMC), with an injection dose of 0.1 ml for each 100 gm intraperitoneally (26). A full-thickness excisional wound was performed by cutting a circle-shaped (2 cm diameter) skin tissue from the dorsum of the rats using sterile scissors, and the wounds were covered with sterile gauze for protection. The experimental animals were divided into 4 groups (n=9/group), as follows: in the first group(control group), the induced skin wounds were left without treatment; in the second group (ChSc group), where the wounds were covered directly with the freeze-dried ChSc; the third group (HUCB-MSCs), in this group the wound edges, were injected with a 500 µl suspension of 3×10^5 of HUCB-MSCs using a specific needle; and the fourth group is (HUCB-MSCs) ChSc, where the ChSc was incubated with 3×10^5 HUCB-MSCs in the culture media (DMEM) (Lonza Bioproducts, Belgium) supplemented with 10% (FBS) (Lonza Bioproducts, Belgium)for 1 hour at 37 C° and then was directly placed on the wounds (8). The wound closure rate was calculated using the measuring ruler to determine the changes in the wound diameter (mm) on the scheduled days 3, 8, and 21. The percent change in wound area was calculated using the following formula (27): [(Area of original wound - the actual wound area)/the original wound area] ×100. The skin tissues were harvested from the experimental rats on days 3, 8, and 21 post wounding (n= 3 for each scheduled day).

Detection of HUCB-MSCs homing and integration into rats' skin by using conventional PCR

HUCB-MSCs homing and integration were detected in the regenerated skin specimens on day 8 post wounding in the HUCB-MSCs group and the (HUCB-MSCs) ChSc group (n=3). The excised skin specimens were homogenized in an ice-cold 50 mM sodium phosphate buffer (pH 7.4) containing 0.1 mM EDTA (Sigma, Aldrich). The resulting supernatant was separated by centrifugation at 1,000 rpm for 20 minutes at 4°C.

The DNA was extracted from the precipitate using the TIAN genomic DNA extraction kit (TIANGEN Beijing, China). The human β-actin gene (a housekeeping gene) was detected using the conventional PCR by the primer kits (BIORON) specific for the human β-actin gene; the forward primer: 5'TGCCCATCTACGAGGGGTATG-3', and the reverse primer: 5'GAAATCGTGCGTGACATTAAGGAG-3'. The amplification protocol was set for the qualitative detection of the human β-actin gene by conventional PCR according to the following steps: incubation at 94°C for 10 minutes, followed by 35 cycles of 94°C for 1 minute, 56°C for 45 seconds, and 72°C for 45 seconds, followed by 72°C for 7 minutes. The PCR products were loaded on 2% Agarose gel (Sigma, Aldrich) with the DNA marker (100-1000 bp). The loaded bands of the Mwt (325 bp) were separated by the submarine gel electrophoresis system (Pharmacia Biotech by SEMKO AB, Sweden) with a submarine chamber (Maxicell, EC360, M-E-C apparatus Co. St Petersburg, FL). The gel image was taken under ultraviolet transillumination (Invitrogen, CA, USA). The electric current was set at 100 mA and 70 volts for 1 hour (28).

Detection of epidermal growth factor receptor (EGFR)-glycan sialyation by the spectrophotometer

The total protein was extracted from the cutaneous wound samples (n=3) from both the control group and the (HUCB-MSCs) ChSc group on day 3 and day 21 post wounding to determine (EGFR) levels at the beginning and the end of the experiment. The extracted protein samples were applied in a standard *in vitro* solid-phase extraction system (SPE) using asialofetuin (ASF) pre-coated plates to determine glycan sialylation levels (29). Briefly, various skin sample lysates were applied to a 96-well microtiter plate. Then the sialyation reaction was initiated by adding CMP-Neu5Ac (Sigma-Aldrich). After routine washing and blocking steps, the sialylated fetuin was allowed to interact with biotinylated plant lectins (MAL-I or SNA) (Vector Laboratories, USA), followed by binding with streptavidin-horseradish peroxidase (Sigma-Aldrich). The negative control of the experiment included only the lectin binding to a sialo-fetuin. At the end of the incubation time, the reaction was developed for 10 minutes by adding 100µl the substrate solution (0.03 % H_2O_2, 2 mg/ml O-phenylenediamine in 0.1 mM citrate buffer, pH 5.5) (Sigma Aldrich) to the skin lysate samples in the wells of the microtiter plate, and then the reaction was terminated with 1M H_2SO_4. The automatic 96-well spectrophotometer (Bio-Rad, USA) was used to measure the absorbance range of the reaction at 492 nm.

Immunoblot assay for determination of (EGFR)α2-6 sialylation profile

Skin sample lysates were incubated with agarose-conjugated SNA lectin, which binds to α2-6 sialylated

proteins. The total sialylated EGFR and particular α2-6 sialylated EGFR proteins were characterized by immunoblots of EGFR (Cell Signaling Danvers, MA, USA), then compared after being treated with neuraminidase and PNGase F enzymes (New England Biolabs) by a wide range of molecular weights (10-200 kDa) protein ladder (Cell Signaling Danvers, MA, USA) to detect the positive α2-6 sialylated EGFR band at (170 kDa) (29).

Histological and immunohistochemical analysis

On each scheduled day, rats from each group were euthanized, and full-thickness skin specimens, including about 3 mm of the skin surrounding the wound, were dissected from each group. The dissected skin specimens were formalin-fixed, treated with ascending gradient concentrations of ethyl alcohol (70%, 90%, 95%, and 100%), and embedded into paraffin blocks (30). Sections of 5 µm thickness were sliced from the paraffin blocks using the microtome, and the tissue sections were stained with Hematoxylin and Eosin (H&E) for general histological analysis. Immunostaining with anti-vascular endothelial growth factor (VEGF) antibody (Cat. No: 6C0529, VEGF A) was performed for detection of the angiogenesis progress (n=3) at day 21 post wounding (31). Masson trichrome staining was performed on tissues on day 21 post wounding to determine the maturity and area percentage of the deposited collagen fibers (n=3). The tissue biocompatibility was studied by staining skin specimens with toluidine blue (n=3) on day 3 and day 21 post wounding for counting mast cells. The stained images were visualized by Olympus BX21 light microscope and captured with a digital Dsc-W800 super steady cyber shot camera (Sony-Japan).

Image analysis and morphometric studies

Qualitative and quantitative analysis of histological and immunohistochemical staining were determined by image analysis software (Image J; 1.51 n, NIH, USA), A standard measurement tool was used for the measurement of the migratory epithelial tongue length (µm), the regenerated epidermis thickness (µm), the granulation tissue thickness (µm), and ChSc pore diameter (µm). Also, the Image J software applied to determine porosity%, mast cells count, in addition to measurements of collagen fibers and VEGF immunostaining area percentage (%).

Statistical analysis

All results were performed by statistical analysis software (IBM SPSS Statistics, version 26, Chicago, USA). Data were normally distributed. Parametric tests were done for comparing means difference using One-way ANOVA, followed by Tukey's test for means multiple comparisons by detecting significance between each group and all other groups. Two-tailed student t-test for comparing two groups. The analyzed data were presented as the mean ± standard error (SEM) and were considered significant when $P \leq 0.05$.

Results

Morphology and immunophenotypic characterization of HUCB-MSCs

The attached HUCB-MSCs on the day 3 of the culture appeared partially elongated with spindle-shaped, while some of the HUCB-MSCs were still rounded. The cells showed mesenchymal characteristics as they attached to the plastic surface of the tissue culture flask (Figure 1a). The immunophenotype characteristics resulted in the cells (85.87%) positively expressing CD105 (Figure 1b).

Integration and homing of HUCB-MSCs within skin tissue

Agarose gel electrophoresis was used to detect the amplified PCR product of the human β-actin gene by imaging under ultraviolet transillumination, and the size of the PCR product was measured based on the DNA markers (Figure 1c, lane M). As expected, human β-actin bands in both rat specimens from the HUCB-MSCs group and (HUCB-MSCs) ChSc group appeared at 325 bp (Figure 1c, lane C, D). As expected, the samples from the control and ChSc groups did not amplify the human β-actin gene (no bands) (Figure 1c, lane A, B). Overall, the results confirmed the integration and homing of HUCB-MSCs within the rat skin tissues.

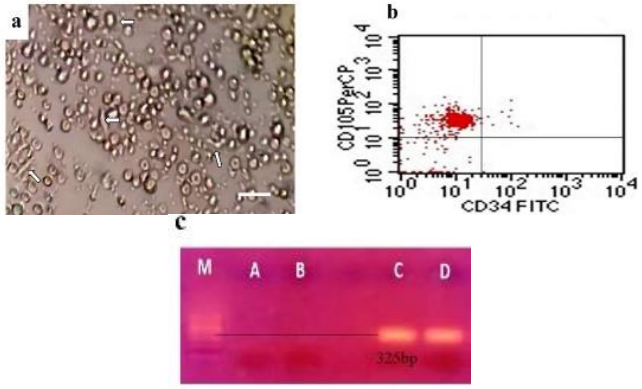

Figure 1: Stem cells differentiation, characterization, and integration (a) Photomicrograph for HUCB-MSCs morphology on the day 3, white arrows: elongated spindle-shaped mesenchymal cells (10x, scale bar=100 µm). (b) Immunophenotypic characterization of HUCB-MSCs. (c) Agarose gel electrophoresis was performed for the integration and homing of HUCB-MSCs by detecting the PCR product of human β-actin bands (325bp): (M; DNA marker 100-1000bp). Negative (lanes A and B) indicate the absence of human β-actin in both control and ChSc treated groups, respectively; while positive (lanes C and D) indicated the presence of human β-actin in both HUCB-MSCs and (HUCB-MSCs) ChSc treated groups, respectively.

Surface characteristics of the Freeze-dried ChSc detected by SEM

SEM examination of ChSc showed a lamellated structure with uniform rounded interconnected pores randomly distributed with different diameters ranging from 25 to 248µm (Figure 2). The porosity percentage of the ChSc was about 75%.

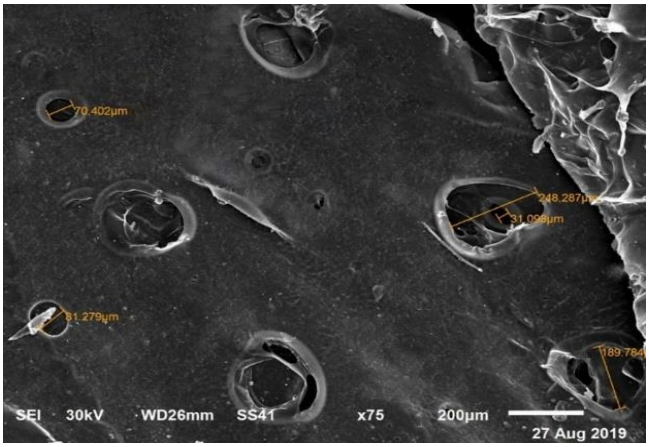

Figure 2: Scaffold characterization (a) SEM image for ChSc illustrating the ultrastructure pores size and distribution within the interconnected lamellated structure; scale bar: 200µm.

Biochemical detection of wound healing and EGFR-sialylation

The sialylation pattern or change in the amount of sialic acid capping terminal glycan chains of EGFR proteins during wound healing is believed to have an essential role in skin maintenance and repair. On biochemical analyses of sialyltransferase activities followed by binding with the biotin-labeled sialic acid lectins, an unusually high binding of SNA (α2-6 sialic acid-specific lectin) (*i.e.,* high expression of α2-6 sialyltransferase) in the (HUCB-MSCs) ChSc group on day 21 post wounding was observed compared to the other groups (Figure 3a). To see if an increased amount of α2-6 sialylated glycans were added to the EGFR or the EGFR contains an excess of α2-6 sialylated glycans during wound repair in the (HUCB-MSCs) ChSc group, skin extracts of the (HUCB-MSCs) ChSc group on day 21 post wounding were allowed to bind with the agarose-conjugated SNA lectin (which binds specifically to α2-6 sialylated glycans). After washing the lectin-agarose beads, the bound sialylated proteins were detected on a western blot probed with the anti-EGFR antibody (Figure 3b-I). Interestingly, the (HUCB-MSCs) ChSc group on day 21 post wounding showed more α2-6 sialylated EGFR than the control group. To confirm the sialylation in the EGFR protein, the skin lysates were treated with neuraminidase first and then carried out the similar steps described above (SNA-agarose binding followed by western blot probed with anti-EGFR antibody). No bands were detected in the neuraminidase-treated extract (Fig. 3b-II), confirming the presence of sialylated glyans in the EGFR. Figure 3b-III shows the glycosylated (total) EGFR (170 kDa) detected from the whole tissue lysates on a western blot probed with an anti-EGFR antibody. Although the EGFR from the (HUCB-MSCs)ChSc group animals contain more α2-6 sialylated glycans, and the molecular weight of the EGFR glycoprotein from the control group seems higher than that from the (HUCB-MSCs) ChSc group indicating the higher glycosylation of the EGFR in the control animals. The higher glycan content in the EGFR from the control animals is not due to the presence of higher *O*-glycans as PNGase F-treated (specifically cuts N-linked glycosylation) samples from both (HUCB-MSCs) ChSc and control groups showed EGFR bands of approximately identical molecular weights (detected by EGFR antibody on western blot) (Figure 3b-IV). To further characterize the location of α2-6 sialylation (in the *N*-glycan, *O*-glycan, or both), the skin lysates were treated with the PNGase F enzyme and then incubated with the SNA-agarose. After washing the lectin-agarose beads, the bound proteins were subjected to a western blot probed with the anti-EGFR antibody. As shown in Figure 3b-V, no bands in the PNGase F-treated samples that went through the SNA-agarose binding were detected on the western blot, indicating that all α2-6 sialic acids are linked only to N-glycans. As expected, the negative controls for the above step, i.e., the cell lysates were treated with the buffer only instead of the PNGase F enzyme and processed identically as described above showed EGFR bands (Figure 3b-VI). Overall, the results demonstrated that the excess α2-6 sialylation, particularly in the EGFR, constitutes vital glycosylation change associated with the wound healing and repair process as observed in the (HUCB-MSCs) ChSc group.

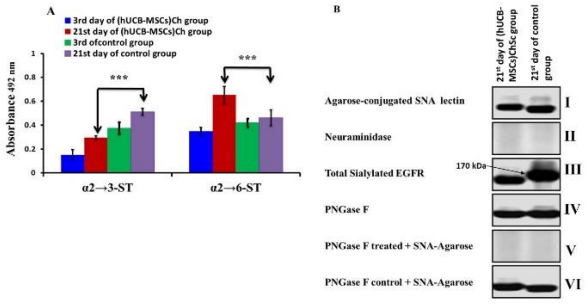

Figure 3: Biochemical detection of sialyltransferase activities and EGFR-sialylation (a) Graphical chart showing sialyltransferase activities in the control and the (HUCB-MSCs) ChSc at days 3 and 21 post wounding. The data were expressed as the mean ± SEM. The difference is considered significant at the P values of ≤0.05, <0.01, and <0.001, indicated by one, two, and three asterisks, respectively; n=3/group. (b) Biochemical evaluation of EGFR-sialylation by the western blot.

The macroscopic examination related to wound closure rate

The macroscopical changes in the wound area of the experimental groups on the scheduled days are shown in Figure 4a. Obvious alternations were noticed in the wound morphology along healing stages; the combined (HUCB-MSCs) ChSc group revealed more efficient gross healing progress than other groups. The wound size was measured during different healing scheduled days 3, 8, and 21 in the four experimental groups, and the percentage of wound reduction was calculated (Figure 4). The wound of the (HUCB-MSCs) ChSc group completely healed at the end of the experiment.

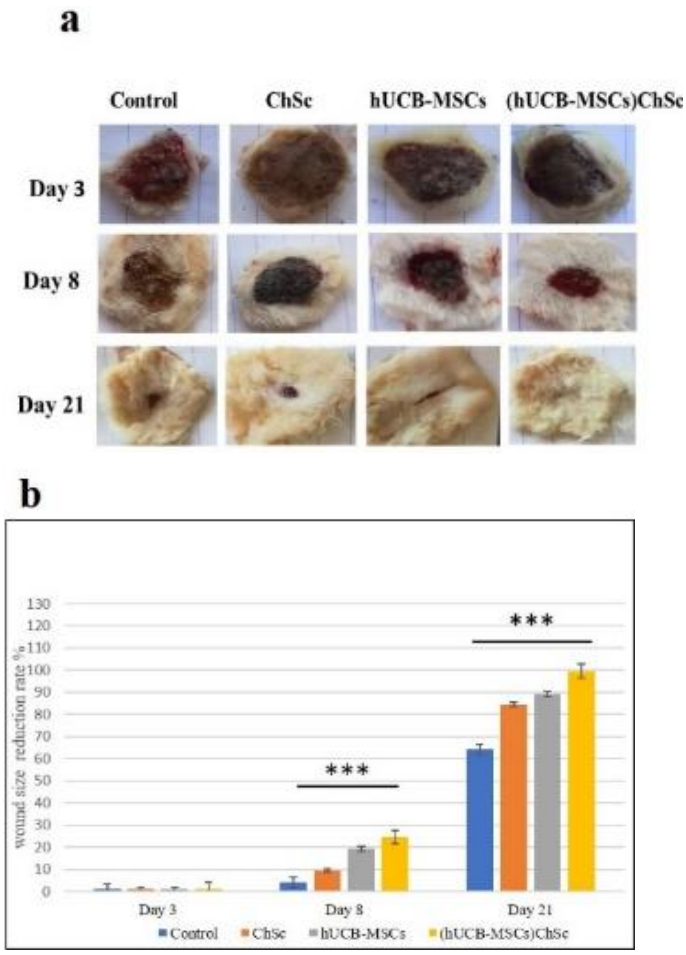

Figure 4: *In vivo* wound healing (a) Representative photo of the gross morphology of the wound bed showing changes in healing progress among different groups on days 3, 8, and 21. (b) Wound reduction rate on days 3, 8, and 21. The data were expressed as the mean ± SEM, and the difference is considered significant at *P ≤ 0.05; n=3/group.

Histological observations

The microscopic observations of the H&E-stained wound sections revealed that, on day 3 post wounding, a slight epidermal thickening with a poorly extended migrating epithelial tongue was observed in all groups except the control group (Figure 5). the migrating epithelial tongue developed more clearer in the (HUCB-MSCs) ChSc group than the other groups (Figure 5a). While in the control group, the migrating epithelial tongue started visibly by day 8 post wounding (Figure 5b). On day 21 post wounding, the migratory epithelial tongue was completely maturated into the prominent epidermis that was completely regenerated in the (HUCB-MSCs) ChSc group. In contrast, the migratory epithelial tongue still grew in the other groups where the epidermis was still not completely developed (Figure 5c). Upon quantitation of the epithelial tongue length and the thickness of the healed epidermis, the (HUCB-MSCs) ChSc group revealed a more efficient healing progress (Figure 6). The mean granulation tissue thickness was obtained by measuring the highest point in the granulation tissue on each scheduled day. The increased thickness of the upwards-growing granulation tissue exhibited a significant difference ($p<0.001$) among the experimental groups throughout the healing stages when compared with the control group (Figure 6). On day 3 post wounding, the thickness of the early granulation tissue in the ChSc and the (HUCB-MSCs) ChSc groups increased compared to the other groups (Figure 5a). The granulation tissue thickness decreased on day 8 post wounding in the (HUCB-MSCs) ChSc group, where the granulation tissue was replaced by the mature dermis with appendages, whereas the granulation tissue in the other groups was still growing (Figure 5b). The microscopic observation for the implanted scaffold in the wound on day 8 in the granulation stage showed in the ChSc group the red-stained lamellated chitosan scaffold embedded within the wound (Figure 7a). Moreover, the day 8 wound section from the (HUCB-MSCs) ChSc group showed the efficient adhesion of the cells on the scaffold structure, where some cells appeared elongated (Figure 7b).

On day 21 post wounding, the wound in the (HUCB-MSCs) ChSc group was closed entirely, and the granulation tissue completely matured and was replaced with the mature collagen III fibers and prominent appendages in the neo-formed dermal layer (Figure 5c). In contrast, the wounds in the other groups were not completely healed and were still in the active granulation phase and the migratory epithelial extended downwards for further appendage formation, as the dermis was not completely maturated (Figure 5c).

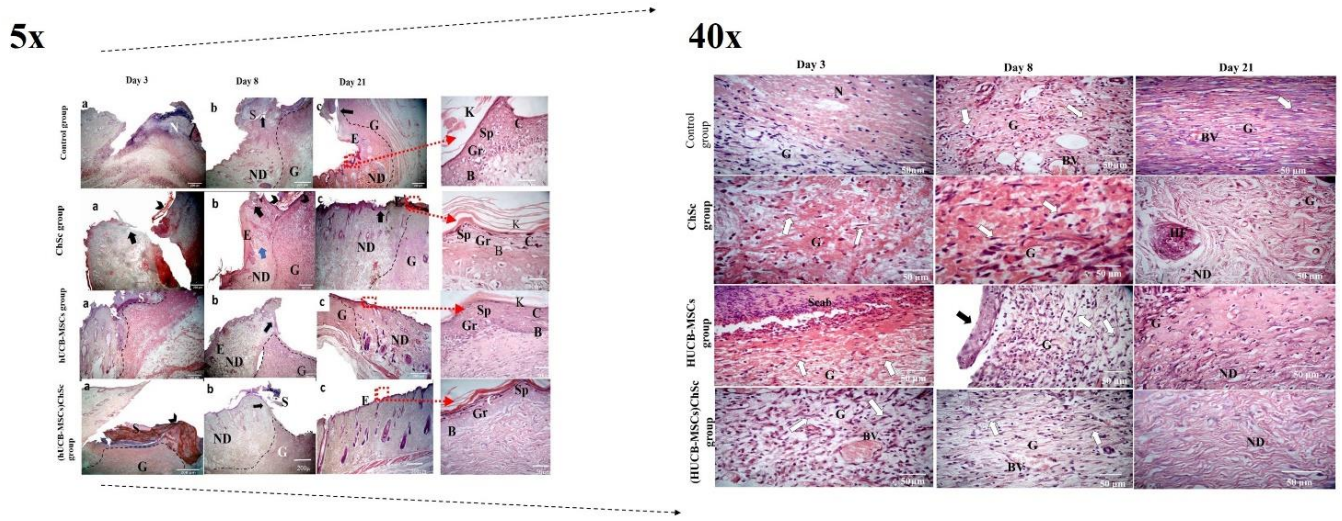

Figure 5: The histological figure of the wound healing progress in the control, ChSc, HUCB-MSCs, and (HUCB-MSCs) ChSc groups on the different scheduled days, stained with H&E. (a) day 3, (b) day 8, and (c) day 21 post wounding, 5x. Scale bar= 200 µm. the red dotted square with an arrow refers to the magnified part of the image (c) showing the microscopic details of newly regenerated tissue, 40x, and the dotted black arrow refers to the magnification of 40x showing maturation of the dermis layer along healing days; scale bar=50 µm. The black dashed line borders the granulation tissue (G), black arrows: the migratory epithelial tongue, black arrowhead: ChSc, blue arrows: migratory epithelia, and white arrows: fibroblasts. (N): necrotic tissue, (S): scab, (E): epithelia, (ND): neo-dermis. (K) keratin layer, (C) stratum corneum, (Gr) stratum granulosum, (Sp.) stratum spinosum, (B) stratum Basale (BV) blood vessel, (HF) hair follicle.

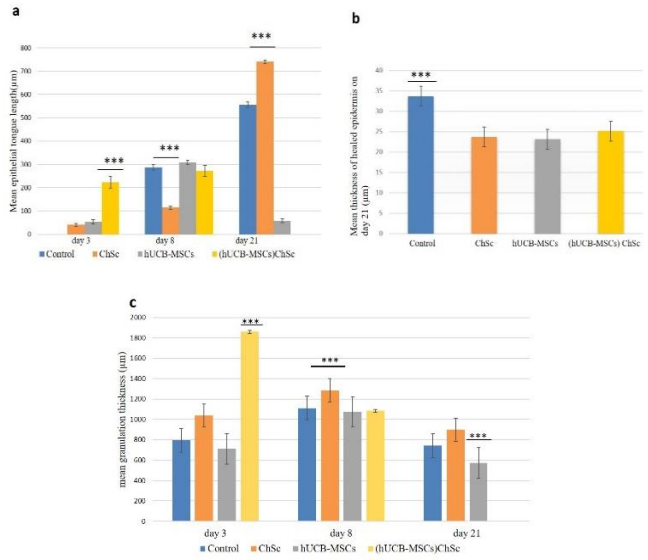

Figure 6: The graphical figures show the difference in the epithelial layer wound healing parameters during healing (a) Mean epithelial tongue length in each group at scheduled days post wounding. (b) Mean thickness of neo-formed epidermis at day 21 post wounding. (c) Mean granulation tissue thickness at days 3, 8, and 21 post wounding from the various groups. The data were expressed as the mean ± SEM. The difference is considered significant at *P ≤ 0.05; n=3/group.

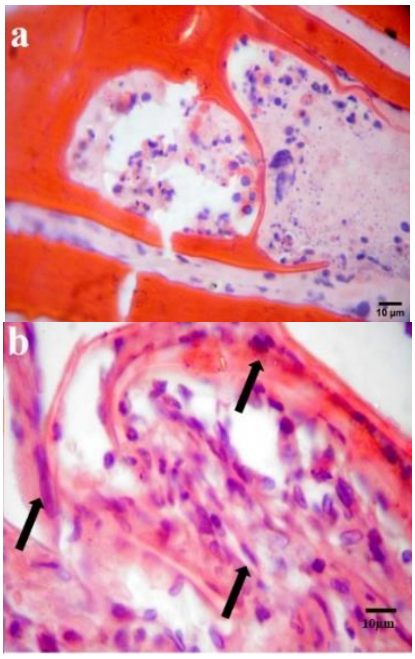

Figure 7: Microscopical figures of the implanted ChSc in the rats' wounds on day 8 stained with H&E (a) Histological micrograph for wound skin covered by ChSc. (b) wound skin covered by ChSc seeded with HUCB-MSCs. Black arrows: elongated adherent cells on the lamellated red scaffold. 100x, scale bar: 10µm.

Immunohistochemical observations

The VEGF immunoreactivity area (%) at the end of the experiment in the (HUCB-MSCs) ChSc group showed a minor immunoreactivity area (%), where the wound was closed entirely, and mature vascularization was observed. The immunoreactivity area (%) was the highest in the control group but moderate in the ChSc, and the HUCB-MSCs groups, respectively, where the wounds were not completely healed and were still in an active state of angiogenesis (Figure 8a). The immune reactivity area (%) of VEGF immunostaining on day 21 post wounding showed a significant difference ($p < 0.01$) in the (HUCB-MSCs) ChSc group when compared to the control group (Figure 8b).

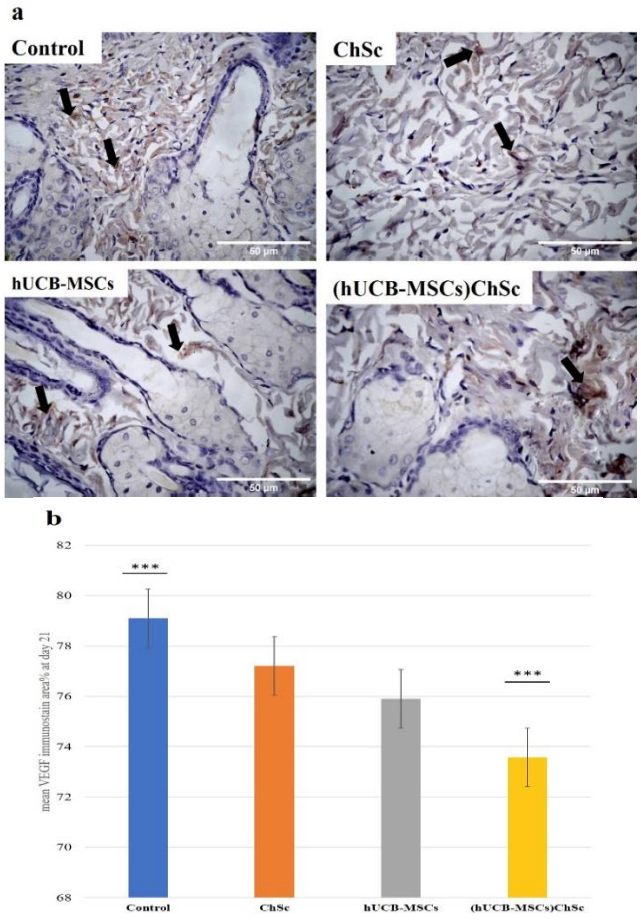

Figure 8: Immunostaining of the wound skin with the anti-VEGF antibody on day 21 post wounding; (a) Showing the control group, ChSc group, HUCB-MSCs group, and (HUCB-MSCs) ChSc group. Black arrows: dense brownish immunoreactive stained vascular endothelial cells. 40 x, Scale bar=50 µm. (b) The graphical figure shows the mean VEGF immunostaining area % in the treated groups compared with the control group at day 21 post wounding. The data were expressed as the mean ± SEM, and the difference is considered significant at *P ≤ 0.05; n=3/group.

Histochemical observations

Masson's trichrome staining was used to detect the organization of the collagen fibers. In the control group, the connective tissue of the papillary layer in the dermis showed fine collagen fiber, while the collagen bundles of the reticular layer in the dermis were thin and loosely arranged. The newly formed immature collagen fibers of granulation tissue occupied a wider area. The (HUCB-MSCs) ChSc and ChSc groups showed more well-formed collagen fibers in the papillary layer, while the dense connective tissue in the reticular layer appeared well-oriented with dense bundles of collagen fibers, which were more than the HUCB-MSCs group (Figure 9a). The area (%) of the collagen fibers was measured on day 21 post wounding and revealed a significant difference among the groups (Figure 9b).

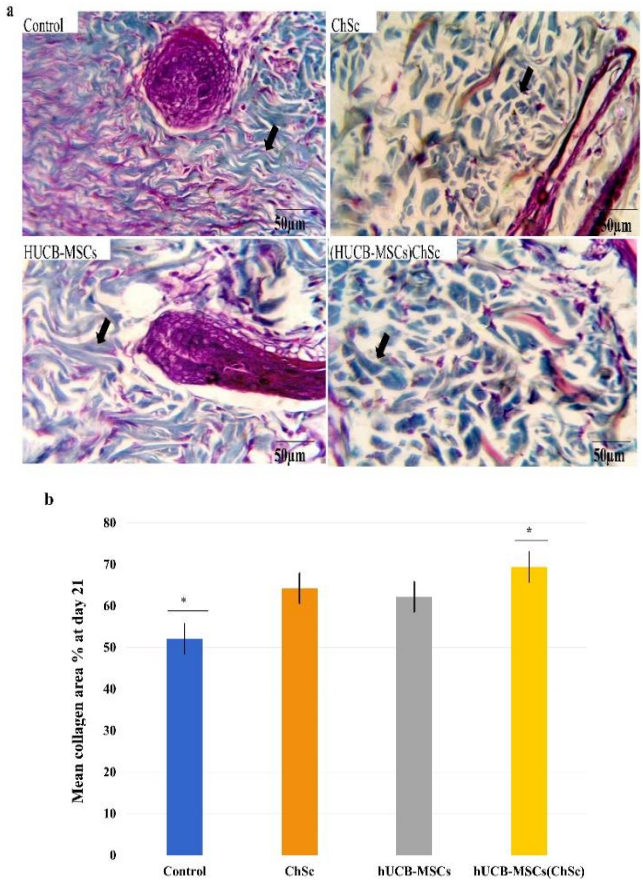

Figure 9: Masson's trichrome staining of the wound skin on day 21 post wounding (a) showing the control group, ChSc group, HUCB-MSCs group, and (HUCB-MSCs) ChSc group. Black arrows: collagen bundles and (G) granulation. 10 x, Scale bar=100 µm. (b) The graphical figure shows the mean collagen area (%) in the treated groups compared with the control group at day 21 post wounding. The data were expressed as the mean ± SEM. The difference is considered significant at *P ≤ 0.05; n=3/group.

The mast cells number at the late stage of healing responded to the quality of the healing and the *in vivo* biocompatibility with the implanted ChSc and cultured HUCB-MSCs. Mast cells were stained with toluidine blue to detect the active degranulated cells (Figure 10 a and b). The mast cells were up-regulated in the treated groups at day 3 post wounding, especially in the (HUCB-MSCs) ChSc group, where the mast cell number was significantly increased compared to the other groups (Figure 10c). On day 21 post wounding, the mast cells were significantly ($P < 0.001$) down-regulated in all treated groups, especially in the combined (HUCB-MSCs) ChSc group, while in the control group number of mast cells remained high number when compared to the day 3 (Figure 10c).

Discussion

The significant finding of the current work is studying the role of the low dose of HUCB-MSCs with chitosan on the cutaneous wound healing process, especially by topical application. Here, we showed the highest healing progress in the combined (HUCB-MSCs) ChSc group. The biochemical investigations of EGFR sialylation revealed that the elevated epidermal growth factor EGF in the (HUCB-MSCs) ChSc group stimulated epidermal regeneration because the EGF promotes cell infiltration and collagen regulation (32,33). In the current study, we also showed that the skin regeneration rate in the ChSc group was lower than both the HUCB-MSCs and the (HUCB-MSCs) ChSc groups. The possible explanation is that when the plain ChSc is filled with the extracellular matrix (ECM) and fibroblasts, ChSc may act as a guiding structure that directs the migrating cells and growing tissue in the direction of the active regenerating tissue (34). This may promote the angiogenesis mechanisms to direct the vascularization towards the scaffold, which was integrated into the ECM. All of this may make the integrated ChSc mimics the histogenesis state of the tissue (35). In the case of (HUCB-MSCs) ChSc, where the ChSc was seeded with MSCs, the ChSc acted more spontaneously as a natural tissue where the seeded HUCB-MSCs enhanced the proliferation and activation of angiogenesis, which increased the degradation rate more than that of the plain ChSc (36). In the previous studies, a large number of HUCB-MSCs (about one or two million cells) that were intradermally administered in a single dose enhanced and accelerated wound healing (16,37).

In this study, the intradermal administration of a low dose of HUCB-MSCs exerted the same levels of wound healing progress as evidenced by decreased scarring and fibrosis and enhanced re-epithelialization and angiogenesis (16,37). This might change the paradigm that the higher the cell count, the better wound healing. Sorg *et al.* (38) mentioned that wound healing could not be established without the epithelial stratification mechanism. In this study, the re-epithelialization was observed at day 3 post wounding in the treated groups earlier than that of the normal healing process in the control group, where the re-epithelialization often started at the proliferation phase after 3-4 days post wounding (39).

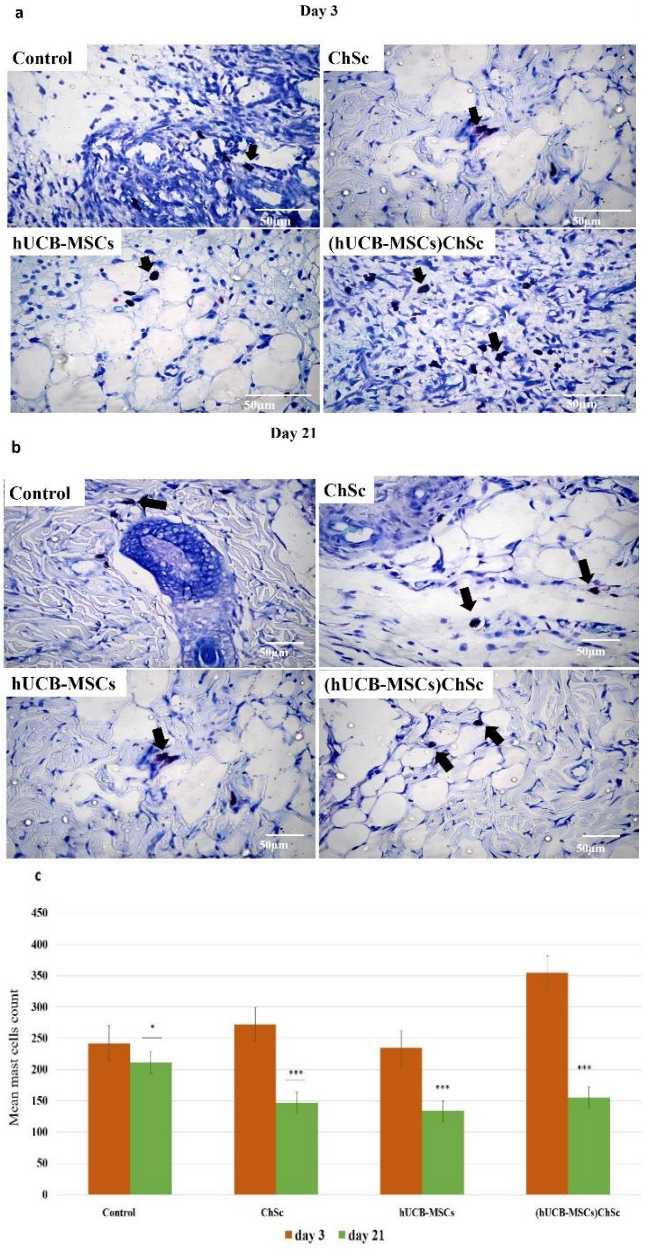

Figure 10: Wound skin stained with toluidine blue (a) day 3 and (b) day 21 post wounding; showing the control group, ChSc group, HUCB-MSCs group, and (HUCB-MSCs) ChSc group. Black arrows: indicate mast cells. 40 x, Scale bar 50 µm. (c) The graphical figure shows the mean number of mast cells counted in a fixed section standard field. The data were expressed as the mean ± SEM, and the difference is considered significant at $*P \leq 0.05$; n=3/group.

The early proliferative phase started on day 3 post wounding in the ChSc group, promoted skin regeneration, well-organized granulation tissue deposition, remodeling, and the active re-epithelialization, which was continued with migrating epithelial tongue extension through day 8 (40,41). It was reported in a previous study that the proliferative stage might fail to be established after the inflammatory stage due to high levels of pro-inflammatory cytokines that aggressively delayed the healing process (42). The current findings indicated that the inflammatory phase declined more rapidly and started re-epithelialization in the early stage in the HUCB-MSCs group, as the HUCB-MSCs resulted in the desired down-regulation of pro-inflammatory cytokines and inflammatory cells (43). Hence, the inflammatory phase declined, followed by increased tissue regeneration and promotion of the healing process (44).

The treated groups, which started early deposition of granulation tissue before day 3 post wounding, would start re-epithelialization earlier. Whereas in the normal wound healing process in the control group, the granulation and remodeling stages occur at day 5 to day 7 post wounding due to the down-regulated activity of inflammatory cells (40,45). This may be due to the role of chitosan and the HUCB-MSCs in promoting and improving collagen secretion by stimulating differentiated fibroblasts for early collagen secretion, which contributes to granulation tissue deposition after the inflammatory stage, almost 3-4 days post wounding (46,47). On day 21 post wounding, the HUCB-MSCs group showed complete epidermal healing, but the dermis layer still appeared in the granulation stage (48). Furthermore, the mature blood vessels were noticed in the remaining granulation tissue and the active migratory epithelia, which migrated downwards from the epidermis into the dermis. This indicated that the regenerated skin was still in an active remodeling state to avoid scar tissue formation with the aid of the HUCB-MSCs (49,50). Although Luo *et al.* (51) suggested that the HUCB-MSCs enhanced the regeneration of dermal appendages, the current findings are considered the slower rate of appendage regeneration in the HUCB-MSCs group might be due to the low injected cellular dose not proportional to the induced large wound area.

Scarring represented the excessive granulation of tissue in the final stage, where the wound healing process was stopped at a particular phase and discontinued shifting to the following stages, and the absence of appendages may occur (52). As shown in a previous study, ChSc, after one weak post-wounding, decreased the expression of the TGF-β, which is responsible for the hypertrophic scarring factor (47). Krasnodembskaya *et al.* (53) reported that the BM-MSCs were accompanied by the secretion of specific immune-modulatory factors, which also regulated fibrotic tissue formation and reducing the scarring of tissue (54).

After day 21 post wounding, the collagen fiber deposition was detected in all experimental groups by Masson trichrome staining. A delay in collagen remodeling was noticed in the control group. These results could be attributed to the initial secretion and deposition of immature collagen type III with thin fibrils, which were replaced later with mature collagen type I of thick and condensed bundles (55-57). In the HUCB-MSCs group, collagen was denser, well remodeled (55). In the ChSc and (HUCB-MSCs) ChSc groups, an efficient deposition and organization of collagen fibers were observed, which might be attributed to the chitosan polymer that enhanced fibroblasts to increase collagen secretion and deposition (58). Therefore, we detected that the ChSc seeded with HUCB-MSCs together, resulted in increased collagen density and well-orientated fibers.

It was previously found that full-thickness wounds treated with BM-MSCs stimulated angiogenesis by expressing high levels of VEGF (59). The ChSc also stimulated VEGF secretion to start the angiogenesis pathway (35). Regarding the current results, the VEGF levels proportionally decreased with the decrease in wound area during healing. Furthermore, in the (HUCB-MSCs) ChSc group, where the wound was completely healed, a lower VEGF level was detected, which might be attributed to the combination of the HUCB-MSCs and the ChSc that enhanced early VEGF stimulation and neo-vascularization (60).

The current finding agrees with the previous studies, which reported that VEGF and neo-vascularization declined after 21 days beyond injection with BM-MSCs (52,57) and Hematopoietic Progenitor Cells (HSCs) (61). This phenomenon may be related to the decline in blood oxygen supply in the healed skin tissue. In the wounded skin, the injury stimulated the up-regulation of VEGF production and a subsequent increase in vascularization during the proliferative phase (62). Hence, the VEGF levels decreased throughout the wound healing, and neo-vascularization stability occurred.

Ud-Din *et al.* (63) found that mast cells in open wounds increased by two folds within two months of the initial count found in non-wounded skin. Mast cells play an essential role in controlling wound healing during the presence of foreign implanted material through the inflammatory response towards the implant (64). At the beginning of the implantation of foreign materials, the mast cells activated and degranulated to release their pro-inflammatory mediators (65). A high increase of degranulated mast cells was noticed after grafting in cases where the tissues were mismatched compared to the non-treated group (65). The increased degranulated mast cells released chemotactic macrophages and neutrophils (66). This mediated the inflammatory response within the implanted material or transplanted tissue and triggered the rejection process consequently (67).

Furthermore, the depletion of mast cells and blocking of the degranulation process delayed the rejection, which supported the graft during the acute inflammatory phase. The current study also observed this phenomenon as the mast cell

count was higher in the (HUCB-MSCs) ChSc group during the inflammatory phase (66). The current finding revealed that, after three weeks beyond complete healing, a dramatic decrease in mast cells in all groups was noticed except in the control group. The (HUCB-MSCs) ChSc group was the least counted due to the combined role of both HUCB-MSCs and ChSc, where the HUCB-MSCs were characterized by suppressing the infiltration of mast cells and deactivating the degranulation mechanism at the end stages of healing (68,69), and the ChSc reduced the inflammatory response of mast cells and decreased neutrophil infiltration (70) within the first week (64). ChSc induced a reduction of mast cell stimuli for fibroblasts; therefore, it displayed a decline in fibroblasts' number and decreased fibrotic tissue formation (71).

Conclusion

The low dose of HUCB-MSCs resulted in significant healing progress compared to the previous studies with a high dose. However, the healing was significantly enhanced when the HUCB-MSCs were seeded with ChSc. Furthermore, the treated groups with either HUCB-MSCs or ChSc reported a noticeable effect on mast cell regulation. The (HUCB-MSCs) ChSc group exhibited a significant healing rate and performance improvement compared to the other groups. This was observed by appropriate collagen deposition without scarring signs, well-formed blood vessels, and EGF increasing, and mast cell numbers regulation during the healing process.

Acknowledgments

The authors would like to thank the department of Histology and Cytology, Faculty of Veterinary Medicine, Zagazig University, Egypt for their support and providing all facilities for this work. And the deepest gratitude to dr. Shaimaa Abd Elsadek Gouhar Assistant Researcher, National Research Centre, Egypt for her aid and support. The authors did not get fund for this work.

Conflict of interest

The authors declare no conflict of interest in connection with this manuscript.

References

1. Wynn TA, Ramalingam TR. Mechanisms of fibrosis: Therapeutic translation for fibrotic disease. Nat Med. 2012;18(7):1028-1040. DOI: 10.1038/nm.2807
2. Karimi K, Odhav A, Kollipara R, Fike J, Stanford C, Hall JC. Acute cutaneous necrosis: A guide to early diagnosis and treatment. J Cutan Med Surg. 2017;21(5):425-37. DOI: 10.1177/1203475417708164
3. Velnar T, Bailey T, Smrkolj V. The wound healing process: An overview of the cellular and molecular mechanisms. J Int Med Res. 2009;37(5):1528-1542. DOI: 10.1177/147323000903700531
4. Dumville JC, Owens GL, Crosbie EJ, Peinemann F, Liu Z. Negative pressure wound therapy for treating surgical wounds healing by secondary intention. Cochrane Database Syst Rev. 2015;(6):CD011278. DOI: 10.1002/14651858.CD011278.pub2
5. Metcalfe AD, Ferguson MWJ. Bioengineering skin using mechanisms of regeneration and repair. Biomaterials. 2007;28(34):5100-5113. DOI: 10.1016/j.biomaterials.2007.07.031
6. Behera SS, Das U, Kumar A, Bissoyi A, Singh AK. Chitosan/TiO2 composite membrane improves proliferation and survival of L929 fibroblast cells: Application in wound dressing and skin regeneration. Int J Biol Macromol. 2017;98:329-340. DOI: 10.1016/j.ijbiomac.2017.02.017
7. Muxika A, Etxabide A, Uranga J, Guerrero P, De La Caba K. Chitosan as a bioactive polymer: Processing, properties, and applications. Int J Biol Macromol. 2017;105(Pt2):1358-1368. DOI: 10.1016/j.ijbiomac.2017.07.087
8. Marei NH, El-Mazny W, El-Shaer A, Zaki KD, Hussein ZS, Abd-El-Samie EM. Enhanced wound healing activity of desert locust (Schistocerca gregaria) vs. shrimp (Penaeus monodon) chitosan-based scaffolds. Int J Biol Macromol. 2017;97:23-33. DOI: 10.1016/j.ijbiomac.2017.01.009
9. Gutha Y, Pathak JL, Zhang W, Zhang Y, Jiao X. Antibacterial and wound healing properties of chitosan/poly (vinyl alcohol)/zinc oxide beads (CS/PVA/ZnO). Int J Biol Macromol. 2017;103:234-241. DOI: 10.1016/j.ijbiomac.2017.05.020
10. Oryan A, Sahvieh S. Effectiveness of chitosan scaffold in skin, bone and cartilage healing. Int J Biol Macromol. 2017;104:1003-1011. DOI: 10.1016/j.ijbiomac.2017.06.124
11. Vijayan AAS, Kumar GSV. PEG grafted chitosan scaffold for dual growth factor delivery for enhanced wound healing. Sci Rep. 2019;9(1):19165. DOI: 10.1038/s41598-019-55214-7
12. Violas P, Abid A, Darodes P, Galinier P, Sales de Gauzy J, Cahuzac J. Integra artificial skin in the management of severe tissue defects, including bone exposure, in injured children. J Pediatr Orthop B. 2005;14(5):381-384. DOI: 10.1097/01202412-200509000-00013
13. Shevchenko RV, James SL, James SE. A review of tissue-engineered skin bio constructs available for skin reconstruction. J R Soc Interface. 20107;(43):229-258. DOI: 10.1098/rsif.2009.0403
14. Mahmood SK, Abdul Razak ISB, Yaseen MT, Yusof LM, Jeber ZK, Gimba F, Zakaria MZAB. 3-D nanocomposite scaffolds: Tissue engineering for bone reconstruction. Iraqi J Vet Sci. 2022;36(2):433-444. DOI: 10.33899/IJVS.2021.130481.1831
15. Jayakumar R, Prabaharan M, Sudheesh Kumar PT, Nair SV. Tamura H. Biomaterials based on chitin and chitosan in wound dressing applications. Biotechnol Adv. 2011;29(3):322-337. DOI: 10.1016/j.biotechadv.2011.01.005
16. Eylert G, Dolp R, Parousis A, Cheng R, Auger C, Holter M, Lang-Olip I, Reiner V, Kamolz L P, Jeschke M G. Skin regeneration is accelerated by a lower dose of multipotent mesenchymal stromal/stem cells—a paradigm change. Stem Cell Res Ther. 2021;12(1):82. DOI: 10.1186/s13287-020-02131-6
17. Secunda R, Vennila R, Mohanashankar AM, Rajasundari M, Jeswanth S, Surendran R. Isolation, expansion and characterization of mesenchymal stem cells from human bone marrow, adipose tissue, umbilical cord blood, and matrix:a comparative study. Cytotechnology. 2015;67(5):793-807. DOI: 10.1007/s10616-014-9718-z
18. Ismail HK, Al-Sabawy RA, Jumaa HJ. Protective effect of placental mesenchymal stem cells on histological changes of pancreas experimentally induced by alloxane in mice. Iraqi J Vet Sci. 2020;34(1):1-8. DOI: 10.33899/IJVS.2020.163563
19. Le Blanc K, Mougiakakos D. Multipotent mesenchymal stromal cells and the innate immune system. Nat Rev Immunol. 2012;12(5):383-96. DOI: 10.1038/nri3209
20. Liao Y, Itoh M, Yang A, Zhu H, Roberts S, Highet AM, Latshaw S, Mitchell K, Van De Ven C, Christiano A. Human cord blood-derived unrestricted somatic stem cells promote wound healing and have therapeutic potential for patients with recessive dystrophic epidermolysis bullosa. Cell Transplant. 2014;23(3):303-17. DOI: 10.3727/096368913X663569

21. Lawrence BJ, Madihally SV. Cell colonization in degradable 3D porous matrices. Cell Adh Migr. 2008;2(1):9-16. DOI: 10.4161/cam.2.1.5884
22. Fong M, Crane JS. Histology, Mast Cells. Treasure Island (FL): StatPearls Publishing;2022. https://www.ncbi.nlm.nih.gov/books/NBK499904/
23. Tcacencu I, Wendel M. Collagen-hydroxyapatite composite enhances regeneration of calvaria bone defects in young rats but postpones the regeneration of calvaria bone in aged rats. J Mater Sci Mater Med. 2008;19(5):2015-2021. DOI: 10.1007/s10856-007-3284-2
24. Ponnaiyan D, Jegadeesan V. Comparison of phenotype and differentiation marker gene expression profiles in human dental pulp and bone marrow mesenchymal stem cells. Eur J Dent. 2014;08(03):307-313. DOI: 10.4103/1305-7456.137631
25. Madihally SV, Matthew HWT. Porous chitosan scaffolds for tissue engineering. Biomaterials. 1999;20(12):1133-1142. DOI: 10.1016/S0142-9612(99)00011-3
26. Michal Z, Katarzyna M, Szymon B, Maurycy P, Tadeusz FK. Comparison of thiopental, urethane, and pentobarbital in the study of experimental cardiology in rats in vivo. J Cardiovasc Pharmacol. 2010;56:38-44. DOI: 10.1097/FJC.0b013e3181dd502c
27. Wu Y, Chen L, Scott PG, Tredget EE. Mesenchymal stem cells enhance wound healing through differentiation and angiogenesis. Stem Cells. 2007;25(10):2648-2659. DOI: 10.1634/stemcells.2007-0226
28. Gouda ZA, Khalifa MEA, Shalaby SM HS. Mechanistic effect of human umbilical cord blood-derived mesenchymal stem cells on the submandibular salivary gland in ovariectomized rats. Biochem Cell Biol. 2018;96(1):57-67. DOI: 10.1139/bcb-2017-0196
29. Badr HA, ElSayed AI, Ahmed H, Dwek MV, Li C, Djansugurova LB. Preferential lectin binding of cancer cells upon sialic acid treatment under nutrient deprivation. Appl Biochem Biotechnol. 2013;171(4):963-974. DOI: 10.1007/s12010-013-0409-6
30. Bancroft J, Layton C, Suvarna S. Bancroft's theory and practice of histological techniques. 7th ed. NY: Churchill Livingstone; 2012.
31. Naruse T, Kawasaki G, Yanamoto S, Mizuno A, Umeda M. Immunohistochemical study of VEGF expression in oral squamous cell carcinomas: Correlation with the mTOR-HIF-1α pathway. Anticancer Res. 2011;31(12):4429-4437. [available at]
32. Wang Z, Qian Y, Li L, Pan L, Njunge LW, Dong L, Yang L. Evaluation of emulsion electrospun polycaprolactone/hyaluronan/epidermal growth factor nanofibrous scaffolds for wound healing. J Biomater Appl. 2016;30(6):686-698. DOI: 10.1177/0885328215586907
33. Wu YY, Jiao YP, Xiao LL, Li MM, Liu HW, Li SH, Liao X, Chen YT, Li JX, Zhang Y. Experimental study on effects of adipose-derived stem cell-seeded silk fibroin chitosan film on wound healing of a diabetic rat model. Ann Plast Surg. 2018;80(5):572-580. DOI: 10.1097/SAP.0000000000001355
34. Lee EJ, Kasper FK, Mikos AG. Biomaterials for Tissue Engineering. Ann Biomed Eng. 2014;42(2):323-337. DOI: 10.1007/s10439-013-0859-6
35. Glim JE, Everts V, Niessen FB, Ulrich MM, Beelen RHJ. Extracellular matrix components of oral mucosa differ from skin and resemble that of fetal skin. Arch Oral Biol. 2014;59(10):1048-1055. DOI: 10.1016/j.archoralbio.2014.05.019
36. Chen Y, Yu Y, Chen L, Ye L, Cui J, Sun Q, Li K, Li Z, Liu L. Human umbilical cord mesenchymal stem cells: A new therapeutic option for tooth regeneration. Stem Cells Int. 2015;2015:1-11. DOI: 10.1155/2015/549432
37. Sierra-Sánchez Á, Montero-Vilchez T, Quinones-Vico MI, Sanchez-Diaz M, Arias-Santiago S. Current advanced therapies based on human mesenchymal stem cells for skin diseases. Front Cell Dev Biol. 2021;9:643125. DOI: 10.3389/fcell.2021.643125
38. Sorg H, Tilkorn DJ, Hager S, Hauser J, Mirastschijski U. Skin wound healing: An update on the current knowledge and concepts. Eur Surg Res. 2017;58(1-2):81-94. DOI: 10.1159/000454919
39. Öztürk F, Ermertcan AT. Wound healing: A new approach to the topical wound care. Cutan Ocul Toxicol. 2011;30(2):92-9. DOI: 10.3109/15569527.2010.539586
40. Gil ES, Panilaitis B, Bellas E, Kaplan DL. Functionalized silk piomaterials for wound healing. Adv Health Mater. 2013;2(1):206-217. DOI: 10.1002/adhm.201200192
41. Tchemtchoua VT, Atanasova G, Aqil A, Filée P, Garbacki N, Vanhooteghem O, Deroanne C, Noël A, Jérome C, Nusgens B, Poumay Y, Colige A. Development of a chitosan nanofibrillar scaffold for skin repair and regeneration. Biomacromolecules. 2011;12(9):3194-3204. DOI: 10.1021/bm200680q
42. Ashcroft GS, Jeong MJ, Ashworth JJ, Hardman M, Jin W, Moutsopoulos N, Wild T, McCartney-Francis N, Sim D, McGrady G, Song X, Wahl SM. Tumor necrosis factor-alpha (TNF-α) is a therapeutic target for impaired cutaneous wound healing. Wound Repair Regen. 2012;20(1):38-49. DOI: 10.1111/j.1524-475X.2011.00748.x
43. Zhang S, Chen L, Zhang G, Zhang B. Umbilical cord-matrix stem cells induce the functional restoration of vascular endothelial cells and enhance skin wound healing in diabetic mice via the polarized macrophages. Stem Cell Res Ther. 2020;11(1):39. DOI: 10.1186/s13287-020-1561-x
44. Wu YS, Chen SN. Apoptotic cell: Linkage of inflammation and wound healing. Front Pharmacol. 2014;5. DOI: 10.3389/fphar.2014.00001
45. Meephansan J, Rungjang A, Yingmema W, Deenonpoe R, Ponnikorn S. Effect of astaxanthin on cutaneous wound healing. Clin Cosmet Investig Dermatol. 2017;10:259-265. DOI: 10.2147/CCID.S142795
46. Baxter RM, Dai T, Kimball J, Wang E, Hamblin MR, Wiesmann WP, McCarthy SJ, Baker SM. Chitosan dressing promotes healing in third-degree burns in mice:Gene expression analysis shows biphasic effects for rapid tissue regeneration and decreased fibrotic signaling. J Biomed Mater Res Part A. 2013;101A (2):340-348. DOI: 10.1002/jbm.a.34328
47. Werner S, Grose R. Regulation of wound healing by growth factors and cytokines. Physiol Rev. 2003;83(3):835-870. DOI: 10.1152/physrev.2003.83.3.835
48. Biazar E, Keshel SH. The healing effect of stem cells loaded in nanofibrous scaffolds on full thickness skin defects. J Biomed Nanotechnol. 2013;9(9):1471-1482. DOI: 10.1166/jbn.2013.1639
49. Rousselle P, Braye F, Dayan G. Re-epithelialization of adult skin wounds: Cellular mechanisms and therapeutic strategies. Adv Drug Deliv Rev. 2019;146:344-365. DOI: 10.1016/j.addr.2018.06.019
50. Fong E, Tzlil S, Tirrell DA. Boundary crossing in epithelial wound healing. Proc Natl Acad Sci. 2010;107(45):19302-19307. DOI: 10.1073/pnas.1008291107
51. Luo G, Cheng W, He W, Wang X, Tan J, Fitzgerald M, Li X, Wu J. Promotion of cutaneous wound healing by local application of mesenchymal stem cells derived from human umbilical cord blood. Wound Repair Regen. 2010; 18(5):506-513. DOI: 10.1111/j.1524-475X.2010. 00616.x
52. Basiouny HS, Salama NM, Maadawi ZM El, Farag EA. Effect of bone marrow-derived mesenchymal stem cells on healing of induced full-thickness skin wounds in albino rat. Int J Stem Cells. 2013;6(1):12-25. DOI: 10.15283/ijsc.2013.6.1.12
53. Krasnodembskaya A, Song Y, Fang X, Gupta N, Serikov V, Lee J-W. Antibacterial effect of human mesenchymal stem cells is mediated in part from secretion of the antimicrobial peptide LL-37. Stem Cells. 2010;28(12):2229-2238. DOI: 10.1002/stem.544
54. Huang MH, Yang MC. Evaluation of glucan/poly (vinyl alcohol) blend wound dressing using rat models. Int J Pharm. 2008;346(1-2):38-46. DOI: 10.1016/j.ijpharm.2007.06.021
55. Seifert AW, Monaghan JR, Voss SR, Maden M. Skin Regeneration in adult axolotls:A blueprint for scar-free healing in vertebrates. PLoS One. 2012;7(4):e32875. DOI: 10.1371/journal.pone.0032875
56. McFarlin K, Gao X, Liu YB, Dulchavsky DS, Kwon D, Arbab AS, Bansal M, Li Y, Chopp M, Dulchavsky SA, Gautam SC. Bone marrow-derived mesenchymal stromal cells accelerate wound healing in the rat. Wound Repair Regen. 2006;14(4):471-478. DOI: 10.1111/j.1743-6109.2006.00153.x
57. Isackson D, Cook KJ, McGill LD, Bachus KN. Mesenchymal stem cells increase collagen infiltration and improve wound healing response to porous titanium percutaneous implants. Med Eng Phys. 2013;35(6):743-753. DOI: 10.1016/j.medengphy.2012.08.002

58. Moura LIF, Dias AMA, Leal EC, Carvalho L, de Sousa HC, Carvalho E. Chitosan-based dressings loaded with neurotensin—an efficient strategy to improve early diabetic wound healing. Acta Biomater. 2014;10(2):843-857. DOI: 10.1016/j.actbio.2013.09.040
59. Gnecchi M, Zhang Z, Ni A, Dzau VJ. Paracrine Mechanisms in adult stem cell signaling and therapy. Circ Res. 2008;103(11):1204-1219. DOI: 10.1161/CIRCRESAHA.108.176826
60. Eming SA, Krieg T, Davidson JM. Inflammation in wound repair: Molecular and cellular mechanisms. J Invest Dermatol. 2007;127(3):514-525. DOI: 10.1038/sj.jid.5700701
61. Zedan ZK, Hassan SA. In vivo study of impact transplantation hematopoietic progenitor cells on induced cutaneous wound healing in rabbits' model. Iraqi J Vet Sci. 2022;36(3):579-589. DOI: 10.33899/IJVS.2021.130949.1899
62. Bao P, Kodra A, Tomic-Canic M, Golinko MS, Ehrlich HP, Brem H. The Role of vascular endothelial growth factor in wound healing. J Surg Res. 2009;153(2):347-358. DOI: 10.1016/j.jss.2008.04.023
63. Ud-Din S, Foden P, Mazhari M, Al-Habba S, Baguneid M, Bulfone-Paus S, McGeorge D, Bayat A. A Double-blind, randomized trial shows the role of zonal priming and direct topical application of epigallocatechin-3-gallate in the modulation of cutaneous scarring in human skin. J Invest Dermatol. 2019;139(8):1680-1690. DOI: 10.1016/j.jid.2019.01.030
64. Farrugia BL, Whitelock JM, Jung M, McGrath B, O'Grady RL, McCarthy SJ, Lord MS. The localization of inflammatory cells and expression of associated proteoglycans in response to implanted chitosan. Biomaterials. 2014;35(5):1462-1477. DOI: 10.1016/j.biomaterials.2013.10.068
65. Ngo Nyekel F, Pacreau E, Benadda S, Msallam R, Åbrink M, Pejler G, Davoust J, Benhamou M, Charles N, Launay P, Blank U, Gautier G. Mast cell degranulation exacerbates skin rejection by enhancing neutrophil recruitment. Front Immunol. 2018;20:9. DOI: 10.3389/fimmu.2018.02690
66. Da Silva EZM, Jamur MC, Oliver C. Mast cell function. J Histochem Cytochem. 2014;62(10):698-738. DOI: 10.1369/0022155414545334
67. Oh W, Kim DS, Yang YS, Lee JK. Immunological properties of umbilical cord blood-derived mesenchymal stromal cells. Cell Immunol. 2008;251(2):116-123. DOI: 10.1016/j.cellimm.2008.04.003
68. Ali HI, Yasssein SN. Immunotherapeutic effect of chitosan and listeriolysin O on *Listeria monocytogenes* infection in mice. Iraqi J Vet Sci. 2021;35:149-155. DOI: 10.33899/IJVS.2021.132332.2082
69. Kim HS, Yun JW, Shin TH, Lee SH, Lee BC, Yu KR, Seo Y, Lee S, Kang TW, Choi SW, Seo KW, Kang KS. Human umbilical cord blood mesenchymal stem cell-derived PGE2 and TGF-β1 alleviate atopic dermatitis by reducing mast cell degranulation. Stem Cells. 2015;33(4):1254-1266. DOI: 10.1002/stem.1913
70. Lee SW, Park HJ, Pei Y, Yeo Y, Hong S. Topical application of zwitterionic chitosan suppresses neutrophil-mediated acute skin inflammation. Int J Biol Macromol. 2020;158:1184-1193. DOI: 10.1016/j.ijbiomac.2020.05.017
71. Thevenot PT, Baker DW, Weng H, Sun MW, Tang L. The pivotal role of fibrocytes and mast cells in mediating fibrotic reactions to biomaterials. Biomaterials. 2011;32(33):8394-8403. DOI: 10.1016/j.biomaterials.2011.07.084

التأثير المشترك للخلايا الجذعية المستخلصة من دم الحبل السري مع قالب الشيتوزان على عملية التئام الجروح الجلدية كاملة السُمك في الجرذان البيضاء

عايده جهاد الشاعر[١]، احمد عوض أبو العطا[١]، هيثم احمد بدر[٢] و دينة محمد الصادق[١]

[١]قسم الأنسجة والخلايا، كلية الطب البيطري، [٢]قسم الكيمياء الحيوية، كلية الزراعة، جامعة الزقازيق، الزقازيق، مصر

الخلاصة

يهدف هذا البحث الي دراسة تأثير الجرعة القليلة من الخلايا الجذعية المستخلصة من دم الحبل السري وقالب الشيتوزان على تحسين عملية التئام الجروح الجلدية في ذكور الجرذان البيضاء. تم استحداث جروح جلدية كاملة السُمك دائرية الشكل قطرها ٢ سم على ظهر ستة وثلاثين من ذكور الجرذان البيضاء، التي تم تقسيمها الي أربع مجموعات: المجموعة الأولى، حيث الجروح تُركت بدون علاج كمجموعة ضابطه. المجموعة الثانية، وفيها تم تغطية الجروح بقالب الشيتوزان المجفد. بينما المجموعة الثالثة تم حقن الجروح بالخلايا الجذعية المستخلصة من دم الحبل السري من خلال الجلد، وفى المجموعة الرابعة تم استخدام قالب الشيتوزان المزروع بالخلايا الجذعية المستخلصة من دم الحبل السري معا لعلاج الجروح. تم رصد مدى تحسن التئام الجروح من خلال الفحوصات النسيجية والنسيجة مناعية والكيميائية الحيوية لكل مجموعات التجارب خلال الأيام ٣، ٨ و٢١ ما بعد العملية. حيث نتجت عنها أن قالب الشيتوزان والجرعة القليلة من الخلايا الجذعية المفصولة من دم الحبل السري، كل على حده، لهما تأثير متوسط على تحسين الالتئام، وبينما أظهرت المجموعة الرابعة ارتفاعاً في معدل الالتئام أكثر من المجموعات الأخرى، حيث تمت ملاحظة ترسيب ملائم للكولاجين بدون أن يسبب ندبات وتنظيم كفء لعدد الخلايا الصارية وجودة تكوين الأوعية الدموية. ونستنتج أن الخلايا الجذعية المفصولة من دم الحبل السري مع قالب الشيتوزان لهما تأثير واضح على تحسين عملية التئام الجروح كما في المجموعة الرابعة، حيث أظهرت معدل وأداء عالي الالتئام للجرح بدون تعقيدات.